Naval Research Laboratory
Washington, DC 20375-5000

NRL Memorandum Report 6277

Correlations Between Micromechanical Features and Material Toughness in HY-100 Steel

D. P. HARVEY II AND M. I. JOLLES

Mechanics of Materials Branch
Materials Science and Technology Division

September 20, 1988

SECURITY CLASSIFICATION OF THIS PAGE

REPORT DOCUMENTATION PAGE

Form Approved
OMB No 0704-0188

1a REPORT SECURITY CLASSIFICATION UNCLASSIFIED	1b RESTRICTIVE MARKINGS
2a SECURITY CLASSIFICATION AUTHORITY	3 DISTRIBUTION / AVAILABILITY OF REPORT Approved for public release; distribution unlimited.
2b DECLASSIFICATION / DOWNGRADING SCHEDULE	
4 PERFORMING ORGANIZATION REPORT NUMBER(S) NRL Memorandum Report 6277	5 MONITORING ORGANIZATION REPORT NUMBER(S)
6a NAME OF PERFORMING ORGANIZATION Naval Research Laboratory 6b OFFICE SYMBOL (If applicable) Code 6382	7a NAME OF MONITORING ORGANIZATION
6c ADDRESS (City, State, and ZIP Code) Washington, DC 20375-5000	7b ADDRESS (City, State, and ZIP Code)
8a NAME OF FUNDING / SPONSORING ORGANIZATION Office of Naval Research 8b OFFICE SYMBOL (If applicable)	9 PROCUREMENT INSTRUMENT IDENTIFICATION NUMBER
8c ADDRESS (City, State, and ZIP Code) Arlington, VA 22217	10 SOURCE OF FUNDING NUMBERS PROGRAM ELEMENT NO: 61153N22 / PROJECT NO: / TASK NO: RR022-01-48 / WORK UNIT ACCESSION NO: DN480-509
11 TITLE (Include Security Classification) Correlations Between Micromechanical Features and Material Toughness in HY-100 Steel	
12 PERSONAL AUTHOR(S) Harvey, II, D.P. and Jolles, M.I.	
13a TYPE OF REPORT Interim 13b TIME COVERED FROM _____ TO _____ 14 DATE OF REPORT (Year, Month, Day) 1988 September 20 15 PAGE COUNT 19	
16 SUPPLEMENTARY NOTATION	

17 COSATI CODES			18 SUBJECT TERMS (Continue on reverse if necessary and identify by block number)
FIELD	GROUP	SUB-GROUP	Fracture surfaces Critical strain energy density

19 ABSTRACT (Continue on reverse if necessary and identify by block number)

Examinations of the fracture surfaces of HY-100 steel tensile specimens with various gage geometries were conducted and the relationships between the fracture features and the material toughness of each specimen as quantified by the critical strain energy density were investigated. It was observed that the microvoid density, the aspect ratio of the microvoids and the percentages of cleavage, microvoid coalescence and ductile tear were related to the critical strain energy density (w_c) obtained from the scale invariant continuum stress-strain curve. The fracture surface and the critical strain energy density were dependent on the triaxiality of the stress state experienced by the specimens which was in turn influenced by the gage geometries of the specimens.

20 DISTRIBUTION / AVAILABILITY OF ABSTRACT ☒ UNCLASSIFIED/UNLIMITED ☐ SAME AS RPT ☐ DTIC USERS	21 ABSTRACT SECURITY CLASSIFICATION UNCLASSIFIED
22a NAME OF RESPONSIBLE INDIVIDUAL Daniel P. Harvey, II	22b TELEPHONE (Include Area Code) (202) 767-9026 22c OFFICE SYMBOL Code 6382

DD Form 1473, JUN 86 Previous editions are obs. ete SECURITY CLASSIFICATION OF THIS PAGE

S/N 0102-LF-014-6603

CONTENTS

CORRELATIONS BETWEEN MICROMECHANICAL FEATURES AND MATERIAL TOUGHNESS IN HY-100 STEEL

INTRODUCTION

There have been a number of studies that have attempted to correlate micromechanical features to global material properties [1-7]. One motivation behind establishing this relationship is to demonstrate some consistency between a given method of evaluating global material properties and the actual physical behavior of a specimen. Previous studies have concentrated on trying to correlate the plane-strain fracture toughness (K_{Ic}) of a material to various fractographic features such as dimple size [1-4], proportions of cleavage and ductile tear [5] and the size of the "stretched zone" [6,7]. The results of these investigations have been successful in showing qualitative relationships between K_{Ic} and the previously mentioned fractographic features. However, attempts to quantify these relationships have been less successful because of substantial scatter in the data. In the present investigation, a study was conducted on HY-100 steel to find possible relationships between fractographic features (i.e. linear microvoid density, microvoid aspect ratios and proportions of microvoid coalescence, ductile tear and cleavage) and the material toughness quantified by the critical strain energy density (w_c) using tensile specimens of various gage geometries.

EXPERIMENTAL PROCEDURE

The specimens used in this study were tensile bars of HY-100 steel with various gage geometries which were from an investigation by Matic, Kirby and Jolles [8]. The composition of the test material is reported in Table 1 and the typical microstructure is shown in Fig. 1. The gage geometries and engineering stress-strain data of these specimens are given in Table 2. The unique stress-strain curve for this heat of HY-100 steel was determined by a hybrid experimental-computational algorithm which uncouples material and geometry influences on observed test specimen deformation [8]. The resulting "continuum stress-strain curve" for the material used in this investigation is shown in Fig. 2. The critical strain energy density for a given specimen is determined by finding the area under this stress-strain curve out to the fracture strain of that specimen. The "global" w_c is determined using the fracture strain defined as $\ln(A_o/A_f)$ and represents the deformation across the fracture surface in an "average" sense. The local w_c for a continuum element at the center of the neck of each specimen, which represents the point of maximum deformation, was calculated using the results of the finite element analyses [8]. Table 3 gives the global fracture strain and the global and local w_c for each specimen. The fracture surfaces of these specimens were characterized using scanning electron microscopy. The following features were measured:

a) the percentages of microvoid coalescence, ductile tearing and cleavage over the entire fracture surface of each specimen,

b) the average linear density of microvoids in the ductile regions of each specimen,

c) the average aspect ratio (height/width) of the microvoids on the fracture surface of each specimen and

d) the percentages of microvoid coalescence, ductile tear and cleavage in the center of the fracture surface of each specimen.

The percentages of the three groups of fracture features were determined by taking scanning electron micrographs of the fracture surfaces at a magnification of 100 X. A grid was then laid over the micrographs and a manual point count was made of the various features. In order to determine the linear microvoid density of the specimens, 1000 X micrographs were taken of randomly selected areas of the fracture surface. Several manual point counts of microvoids across a given distance were made. From these counts, average values were computed. Aspect ratios were determined by taking

Manuscript approved August 9, 1988.

two micrographs (one at zero degrees tilt, the other at six degrees tilt) of several randomly selected areas at a magnification of 1000 X. Once the micrographs were taken, the height was determined by the parallax stereo-pair method [9] and the width was measured from the micrograph at zero degrees tilt. From these measurements, the average aspect ratio for each specimen was calculated. The micrographs shown in Figs. 3a and 3b are a typical stereo-pair used to determine linear microvoid densities and void aspect ratios. The observed fractographic features were then correlated with the appropriate (local or global) value of w_c.

RESULTS AND DISCUSSION

The damage incurred by a material specimen that undergoes mechanical deformation can be attributed to two basic mechanisms. The first of these is fracture which involves the breaking of atomic bonds along specific crystallographic planes or along interfacial boundaries in a material. The second mechanism is material flow which is generally accomplished by slip due to dislocation motion. The energy exerted by a material specimen subjected to loading is determined by the relative proportions of these mechanisms. The energy associated with fracture may be expressed as:

$$E_{frac} = (\int \sigma_{frac} dA) d_{frac} \tag{1}$$

where σ_{frac} is the normal stress required for bond separation, A is the area over which the stress acts and d_{frac} is the distance required to accomplish this separation. The energy associated with flow may be similarly expressed as:

$$E_{\text{flow}} = (\int \sigma_{\text{flow}} dA)\, d_{\text{flow}} \tag{2}$$

where σ_{flow} is the resolved shear stress required for dislocation motion and d_{flow} is the total distance traveled by all of the dislocations in the specimen. In most engineering materials, the stresses involved in fracture are generally larger than those involved in flow, but usually not by more than an order of magnitude or so. On the other hand, d_{flow} is often several orders of magnitude larger than d_{frac}; consequently, the energy associated with flow is much greater than the energy associated with fracture. Thus it follows that the deformation energy of a material specimen subjected to loading is dependent largely on its ability to flow. If flow is able to occur, then a large amount of energy is required to fail a specimen. If flow is restricted in some way, then the required amount of energy to cause failure in a specimen is decreased.

Certain fractographic features are associated with a particular failure mechanism. Flat facets and river patterns are associated with fracture, microvoid coalescence and ductile rupture are associated with flow and ductile tearing is due to come combination of flow and fracture. Therefore, the relative amounts of material flow and fracture (and thus the material toughness) should be reflected in the fracture surface of a failed specimen. Figures 4 and 5 are representative of the fracture surfaces of the specimens with the largest and smallest global critical strain energy densities respectively. In Figure 4, the fracture surface is predominantly microvoid coalescence while in Figure 5, larger proportions of ductile tear and cleavage are visible. These observed differences in the fracture surfaces were quantified in terms of the percentage of the fracture surface characterized by either microvoid coalescence, ductile tear or cleavage. These values were then plotted vs. the global critical strain energy densities as shown in Figure 6 which indicates that the percentage of fracture sites characterized by microvoid coalescence increases proportionally with the global w_c. This, as well as the decrease in the percentage of cleavage sites as the global w_c increases is consistant with the changes in damage mode that would be expected as the energy to failure of a specimen increases.

Figure 7 shows the relationships between the percentages of microvoid coalescence, ductile tear and cleavage and the local continuum w_c at the center of the HY-100 steel tensile specimens. Immediately apparent is that the correlations between material toughness and fracture mode exist on a local scale as well as on a global scale. Also of interest is the cross-over in the dominant mode of fracture from cleavage to microvoid coalescence as the local w_c increases. In previous analyses [8], it was found that the specimen with the lowest local w_c had an initial stress condition that was triaxial at the center whereas the other three specimens had initial stress states which were uniaxial. Fractographic observations revealed that the specimen with an initially triaxial stress at the center failed primarily by cleavage at the center while the specimens which were initially uniaxial failed predominantly by microvoid coalescence at the center.

As shown in Figure 8, the linear microvoid density on the fracture surfaces of these specimens increases in proportion to the global critical strain energy density. It is generally accepted that microvoids nucleate primarily at second phase particles [10,11] when a critical value of normal stress is exceeded. In a given material specimen, there is a population of second phase particles which vary in both size and shape. This variation in particle geometry leads to a variation in the critical microvoid nucleation stress from particle to particle [12]. All of the tensile specimens used in this study were from the same heat of HY-100 steel. Consequently, they all had the same volume fraction of and all had similar size and shape distributions of second phase particles. Therefore, the observed differences in microvoid density must be due to changes in the stresses acting at the particle-matrix interfaces. LeRoy et al. [13] have given the critical value of normal stress at void nucleation as:

$$\sigma_c = \sigma_{loc,\,c} + \sigma_m \tag{3}$$

where σ_m is the hydrostatic stress and $\sigma_{loc,\,c}$ is the local stress due to incompatibility strains between the matrix and the second phase particle at void nucleation. It then follows that prior to void nucleation, the normal stress acting at the particle matrix interface is given by:

$$\sigma = \sigma_{loc} + \sigma_m \tag{4}$$

where σ_{loc} is again defined as the local stress due to incompatibility strains, but prior to void nucleation. σ_{loc} is proportional to the dislocation density at the particle which in turn is dependent on the magnitudes of the resolved shear stresses present in a specimen.

A triaxial stress state is one of a number of metallurgical and mechanical factors which can restrict flow in a material specimen. It is well established that the triaxiality of the stress state experienced by a material specimen is affected by the geometry of that specimen. As the thickness of a specimen is increased, there is an increase in the transverse stresses needed to maintain continuity between individual volume elements. The maximum resolved shear stress in a material specimen is given by:

$$\tau_{max} = (\sigma_{axial} - \sigma_{trans})/2 \tag{5}$$

where τ_{max} is the maximum resolved shear stress, σ_{axial} is the normal stress in the axial direction and σ_{trans} is the minimum transverse stress. As the specimen geometry is altered to increase σ_{trans}, τ_{max}, the driving force behind dislocation motion, is decreased which in turn decreases the dislocation density and σ_{loc}. Therefore, the observed differences in microvoid density are due to the phenomenon that as the stress triaxiality increases, the magnitudes of the resolved shear stresses decrease, thereby lowering the normal stress acting at particle-matrix interfaces and attaining the critical stress needed

for microvoid nucleation for a smaller percentage of the population of second phase particles. This decrease in the resolved shear stresses also results in a decrease in material flow which results in a lowering of the energy needed for specimen failure.

Figure 9 shows that the average aspect ratio (height/width) of microvoids increases with an increase in the global w_c. Under uniaxial loading, microvoids grow mainly in the tensile direction; a triaxial stress is required to induce any appreciable lateral microvoid growth [13]. The proportional increases in the aspect ratio and in the global w_c are consistant indications of the decrease in the degree of the triaxiality of the stress state as the gage geometry of the specimens is changed. The effects of specimen geometry on fracture morphology have also been observed in HSLA steels [14]. In that investigation it was noted that the aspect ratio of the dimples in tensile specimens was much greater than the aspect ratio of dimples in three point bend specimens for a given steel. This difference was attributed to the higher stress triaxiality at the crack tip of the three point bend specimens. Also apparent from viewing Figure 9 is that the range of aspect ratios generally increases with an increase in global w_c. This is the case because void nuclation occurs over a range of energies and the first voids nucleated are already growing as other voids are nucleated [13]. As the global w_c increases, there is a greater range of energies available over which void nucleation and growth can occur, so the first voids nucleated have more opportunity to grow before the last voids are nucleated.

SUMMARY AND CONCLUSIONS

The consistent relationships observed between micro-mechanical features and material toughness quantified by critical strain energy density in this investigation strongly suggest that the fracture surface of a failed specimen is not a random variable remotely related to the global properties of that specimen, but rather is a direct function of the response of a material to mechanical deformation. The results of this investigation show that the fracture surface of a material can be altered by changing the geometry of a material specimen, thereby changing the triaxiality of the stress state which affects the plastic flow behavior of a specimen. This indicates that the mechanisms of material damage are not solely a material response but are also dependent on the geometry and loading conditions of a specimen. In this study, it was also found that the relationships between the various observed micromechanical features and the critical strain energy density were all first-order linear. This excellent correlation between the actual physical behavior of the specimens and the analytical description of that behavior seems to indicate that the critical strain energy density is an accurate measure of the plastic deformation characteristics of a material specimen and also indicates that the continuum stress-strain curve is an accurate description of the flow behavior of a material. These observations also demonstrate that strain energy density is a parameter which is able to quantitatively link material response to mechanical loading on the macroscopic and microscopic levels.

REFERENCES

1. A.J. Birkle, R.P. Wei and G.E. Pellissier, Analysis of plane strain fracture in Ni-Cr-Mo alloys. *ASM Trans.* 59, p. 981 (1966).

2. W.A. Spitzig et al., A fractographic analysis of the relationships between fracture toughness and surface topography in ultrahigh-strength steels. *ASTM STP* **436**, p. 17 (1968).

3. C.D. Beachem and R.M.N. Pelloux, Electron Fractography - A tool for the study of micromechanisms of the fracturing process. *ASTM STP* **381**, p. 210, (1965).

4. W.W. Gerberich and C.E. Hartbower, Some Observations on Dimple Size in Cyclic-Load-Induced Plane-Stress Fracture. *ASM Trans.* 61, p. 184 (1968).

5. J.M. Barsom and J.V. Pellegrino, Relationship Between KIc and Plane Strain Tensile Ductility and Microscopic Mode of Fracture. # *Eng. Frac. Mech.* 5, p. 209 (1973).

6. R.K. Pandey and S. Banerjee, Studies on Fracture Toughness and Fractographic Features in Fe-Mn Base Alloys. *Eng. Frac. Mech.* 5, p. 965 (1973).

7. D. Broek, Correlation Between Stretched Zone Size and Fracture Toughness, *Eng. Frac. Mech.* 6, p. 173 (1974).

8. P. Matic, G.C. Kirby III and M.I. Jolles, The Relationship of Tensile Specimen Size and Geometry Effects to Unique Parameters for Ductile Materials, NRL Memorandum Report 5936 (1987).

9. B. Hudson, The application of stereo-techniques to electron micrographs. *J. of Microscopy* 98, p. 396 (1973).

10. D. Broek, Some Contributions of Electron Fractography to the Theory of Fracture, Int. Met. Rev. (No. 185) 19, p. 135 (1974).

11. J. Gurland and J. Plateau, The Mechanism of Ductile Rupture of Metals Containing Inclusions. *Trans. ASM* 56, p. 442 (1963).

12. A.W. Thompson, The Relation Between Changes in Ductility and in Ductile Fracture Topography: Control by Microvoid Nucleation, Acta Met. 31, p. 1517 (1983).

13. G. LeRoy, J.D. Embury, G. Edward and M.F. Ashby, A Model of Ductile Fracture Based on the Nucleation and Growth of Voids, Acta Met. 29, p. 1509 (1981).

14. M.N. Bassim, R.J. Klassen, M.R. Bayoumi and H.G.F. Wilsdorf, Fracture Topography of HSLA Steels, *Mat. Sci. and Eng.* 92, p. 107 (1987).

TABLE 1: Typical composition of HY-100 steel

C	Mn	P	S	Cu	Si	Ni	Cr	Mo	V	Ti
0.15	0.33	0.007	0.017	0.17	0.26	2.71	1.51	0.41	0.003	0.003

(balance Fe)

TABLE 2—Gage Geometries, Engineering Stress-Strain and Reduction of Area Data

Specimen	Gage Dia. (in.)	Gage Length (in.)	Yield Strength (ksi)	Ultimate Tensile Strength (ksi)	elong	RA
A	0.3	2.0	106.0	119.0	0.1462	0.7298
B	0.3	0.5	104.5	119.0	0.2500	0.6888
C	0.7	2.0	108.5	122.0	0.3890	0.5954
D	0.7	0.5	112.5	127.0	0.4551	0.4738

TABLE 3—Global Fracture Strain, Global w_f and Center Point Continuum w_c

Specimen	$\ln (A_o/A_f)$	Global w_f (in-lbs/in^3)	Center Point Continuum w_c (in-lbs/in^3)
A	1.3088	186,000	158,900
B	1.1674	160,000	167,170
C	0.8984	124,000	174,340
D	0.6421	90,000	128,860

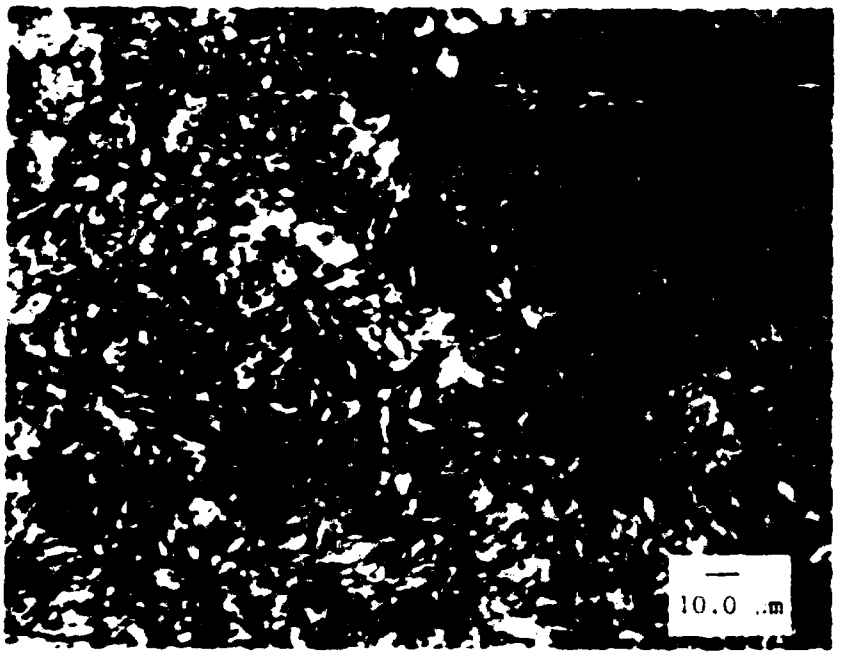

Fig 1 -Typical microstructure of the test material

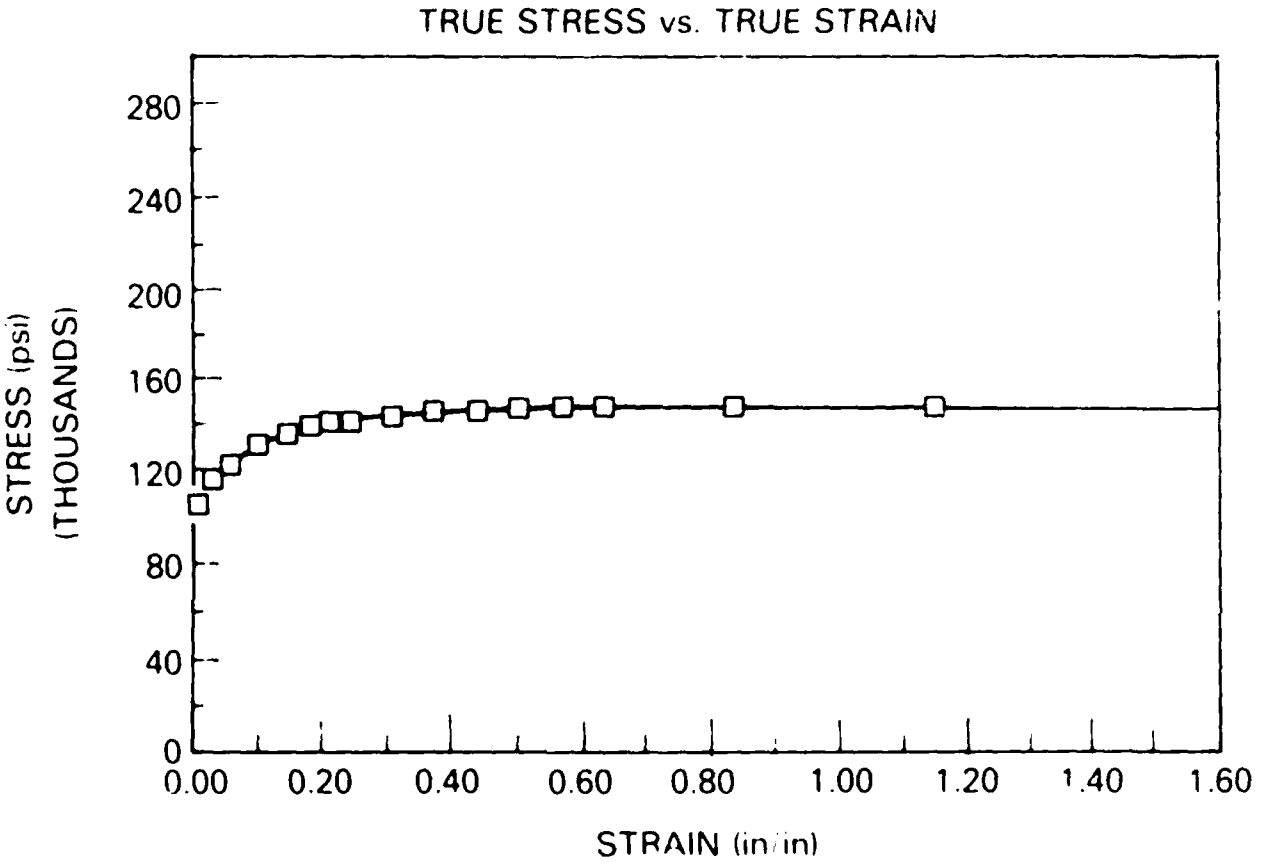

Fig. 2 Continuum stress strain curve for HY 100 steel test material

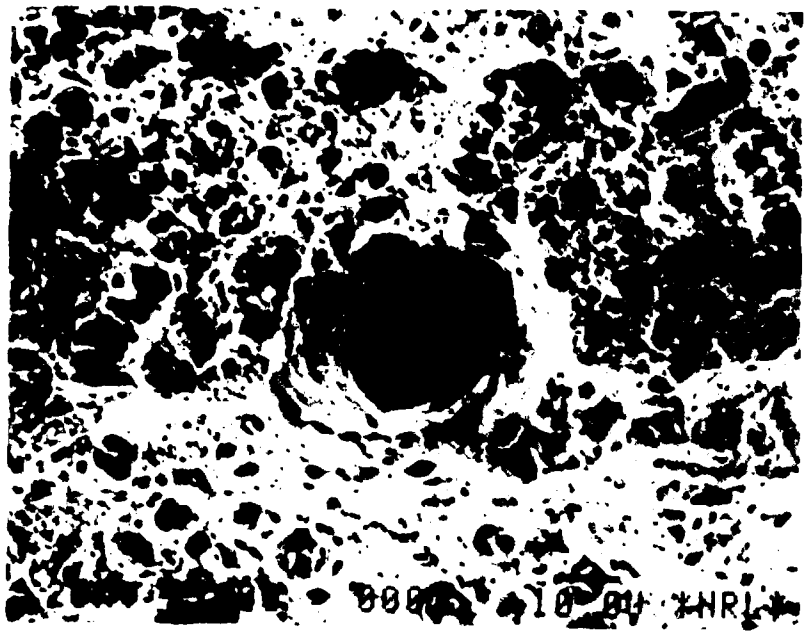

(a)

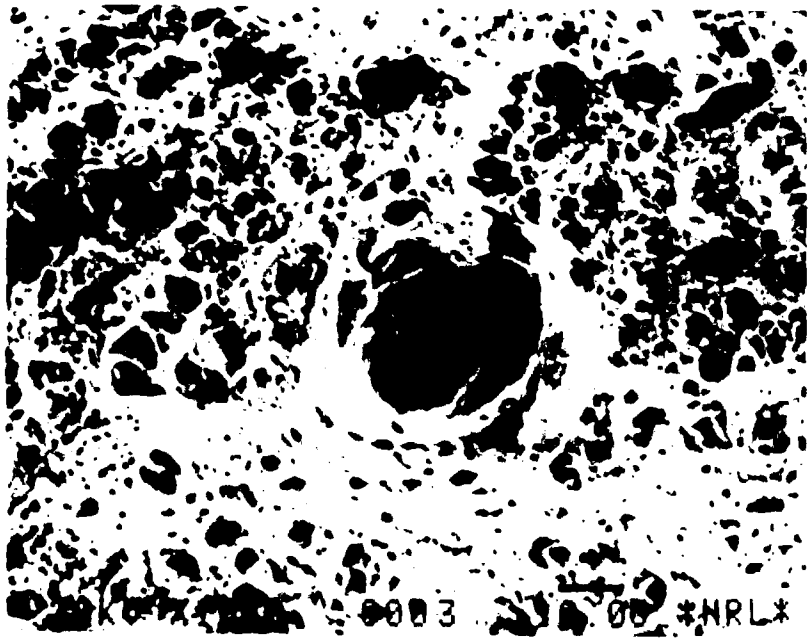

(b)

Fig. 3(a) and (b)—Typical scanning electron microscope stereo-pair of the fracture surface of a HY-100 steel tensile specimen (1000 X, six degrees tilt between pair)

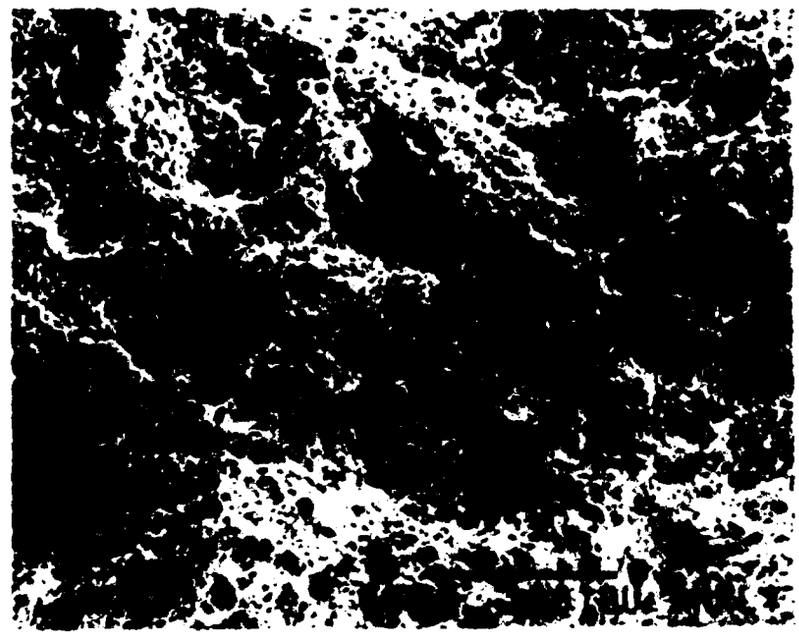

Fig. 4—Fracture surface of HY-100 steel specimen with global w_c = 186,000 in-lbs/in^3

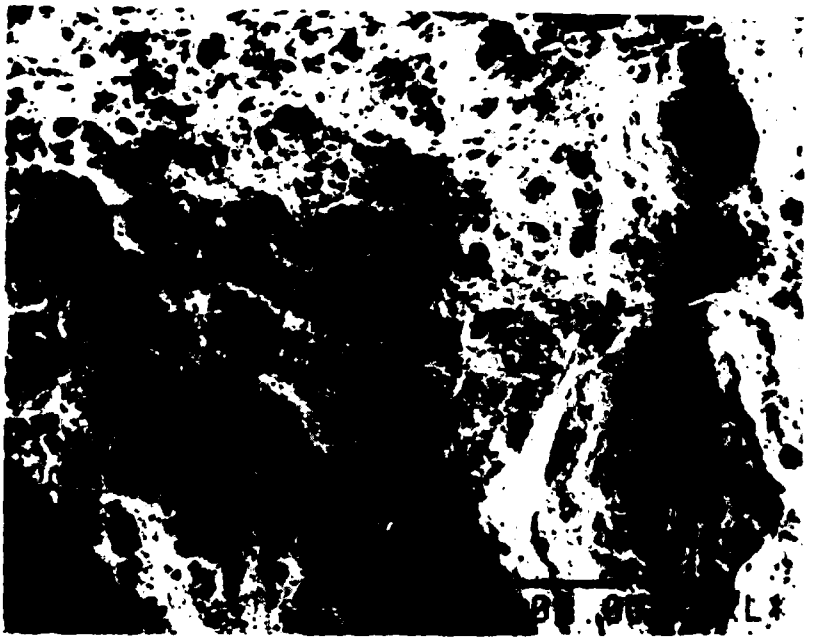

Fig. 5—Fracture surface of HY-100 steel specimen with global w_c = 90,000 in-lbs/in^3

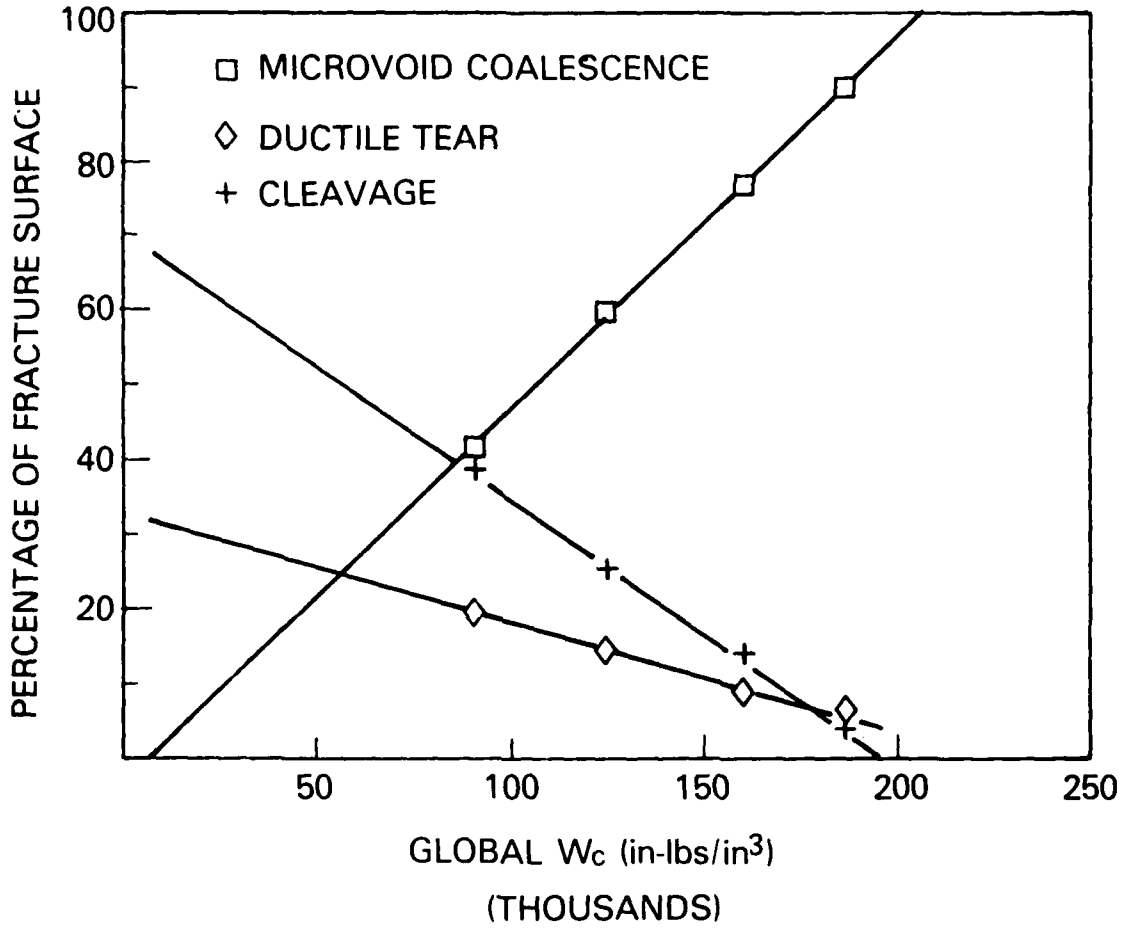

Fig. 6—Percentages of fracture modes as a function of global w_c

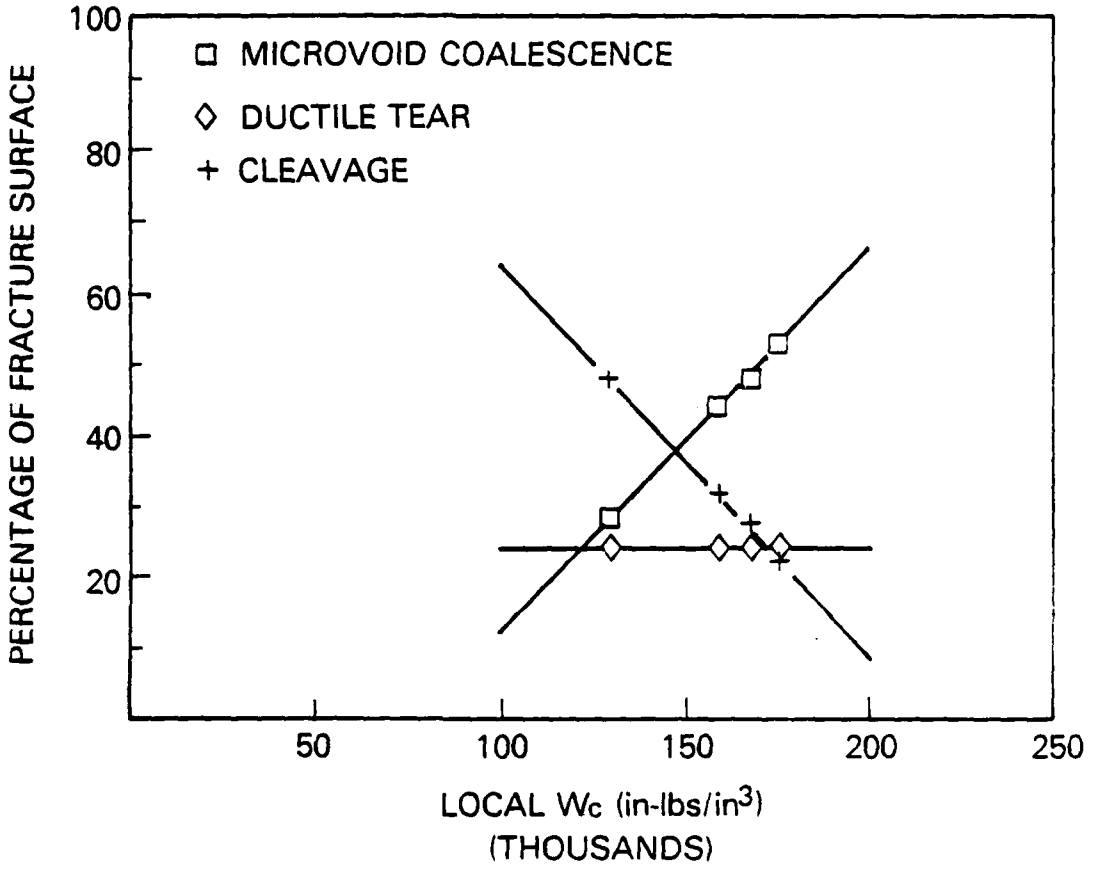

Fig. 7—Percentages of fracture modes around center of specimen as a function of local continuum w_c

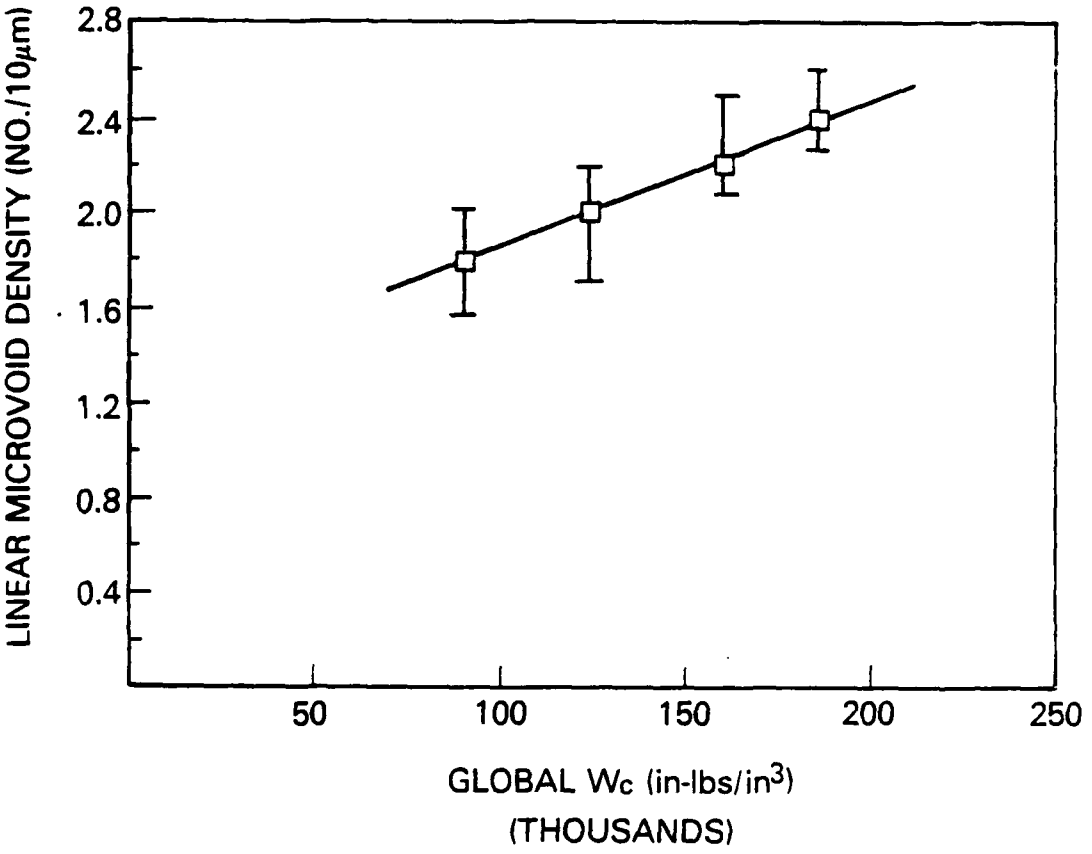

Fig. 8—Linear microvoid density as a function of global w_c

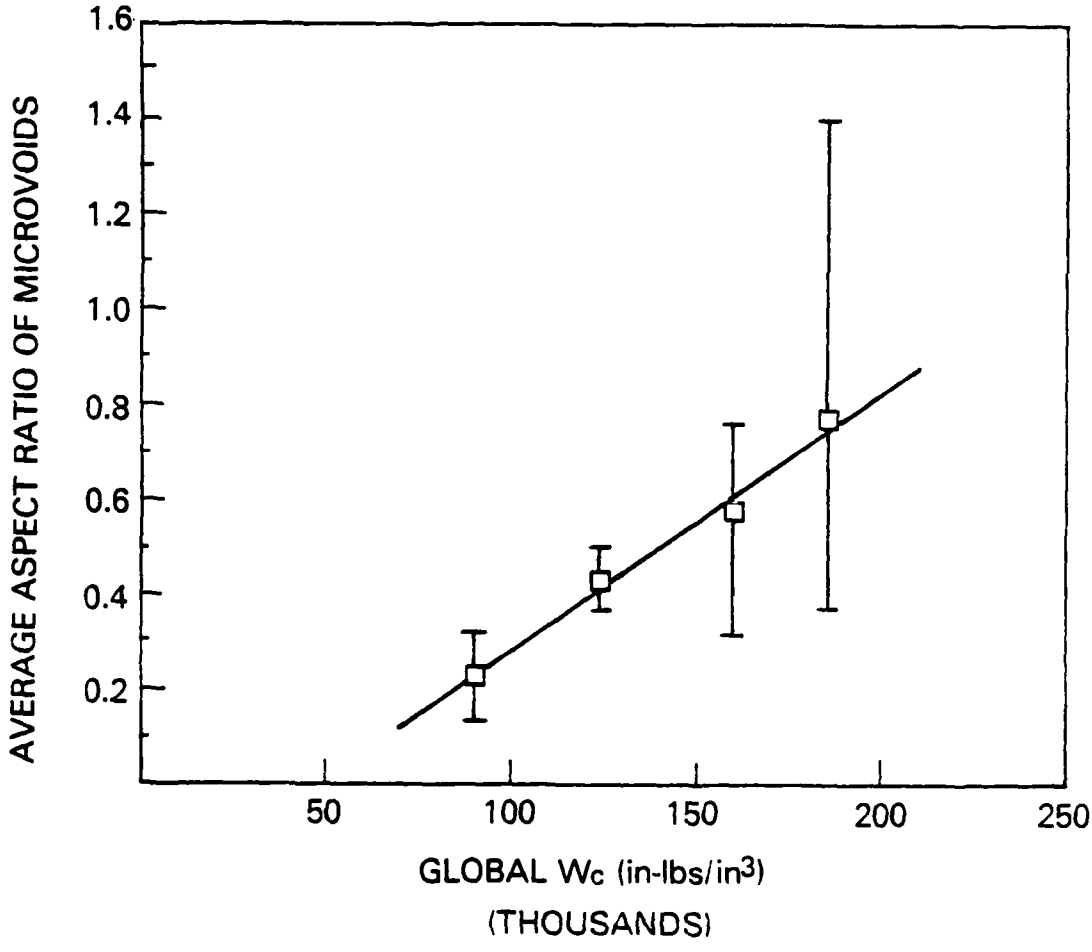

Fig. 9—Average aspect ratio of microvoids as a function of global w_c